Journal of ELECTRONIC MATERIALS, Vol. 47, No. 12, 2018
https://doi.org/10.1007/s11664-018-6644-4

Role of Graphene-Doped Organic/Polymer Nanocomposites on the Electronic Properties of Schottky Junction Structures for Photocell Applications

OSMAN ÇIÇEK ,[1,5] SERHAT O. TAN,[2,6] HÜSEYIN TECIMER,[3,7] and ŞEMSETTIN ALTINDAL[4,8]

1.—Department of Electrical and Electronics Engineering, Faculty of Engineering and Architecture, Kastamonu University, Kastamonu, Turkey. 2.—Department of Electric and Energy, TOBB Tech. Sciences Vocational School, Karabuk University, Karabük, Turkey. 3.—Department of Mechatronics Engineering, Faculty of Technology, Karabük University, Karabük, Turkey. 4.—Physics Department, Faculty of Sciences, Gazi University, Ankara, Turkey. 5.—e-mail: ocicek@kastamonu.edu.tr. 6.—e-mail: serhatorkuntan@karabuk.edu.tr. 7.—e-mail: huseyintecimer@karabuk.edu.tr. 8.—e-mail: altundal@gazi.edu.tr

In this study, the current–voltage characteristics of non-doped and distinct graphene (Gr)-doped polyvinyl alcohol (PVA) interlayers in metal/organic polymer semiconductor type Schottky junction structures (SJSs) were investigated on both forward and reverse biases under distinct levels of illumination. The distinct doping concentration ratios (1%, 3% and 7%) of the Gr added to the PVA interlayers were compared by taking into account the basic electrical parameters, such as saturation current (I_o), ideality factor (n), barrier height (Φ_{Bo}), series (R_s) and shunt resistance (R_{sh}). The 7% Gr-doped structure displayed the lowest I_o values at zero bias. Moreover, the results indicated that the 7% Gr-doped PVA decreased the n value but increased the Φ_{Bo} value compared with values associated with structures that have different doping concentrations. In terms of quality and reliability, the R_s and R_{sh} values of the SJSs were obtained using Ohm's law and Cheung's functions, and the 7% Gr-doped structure eventually displayed more uniformly distributed and lower R_s values and the highest R_{sh} values. Consequently, the 7% Gr-doped structure had better overall quality because of its superior electrical properties compared with structures that have other doping concentrations. Therefore, the 7% Gr-doped structure can be used as a photodiode in electronic devices.

Key words: Graphene, organic polymer nanocomposites, photovoltaic, *I–V* characteristics, basic electronic properties

BACKGROUND

Schottky junction [i.e., metal (M)–semiconductor (S)] structures (SJSs) are the basic components in integrated circuits and play a major role in the improvement of integrated circuit performance.[1] The primary goal for SJSs is to attain superior performance and decrease the cost of devices by modifying conventional SJSs.[2] These structures have been thoroughly investigated by the scientific community with respect to their electrical and photovoltaic behaviours. In the last two decades, many scientists have researched the placement of organic polymer layers between the M and S layers to improve the efficiency of electronic devices because of their unique properties, including electrical behaviours, low-cost manufacturing, large area, flexibility and ease of use.[3–5] Although non-doped organic polymer materials normally have

(Received January 31, 2018; accepted September 1, 2018; published online September 19, 2018)

poor conductivity, their potentials can be effectively increased by suitable dopant materials, such as M ions or Gr.[4,6–8] Shirakawa et al.[9] discovered conducting polyacetylene films in 1977, and these intrinsic electrically conductive polymers became a major fabrication material owing to their unique electrical, optical and chemical properties, thus leading to their wide implementation.

Metal/organic polymer semiconductor (MPS)-type SJSs with a thin, interfacial organic polymer layer, such as polyaniline, poly(alkylthiophene), polypyrrole, polythiophene, poly(3-hexylthiophene) or polyvinyl alcohol (PVA), have been studied by many scientists. PVA nanofillers have proven to be particularly interesting because of certain matchless features and their practical applications in electronic components.[10,11] However, PVA generally displays poor electrical conductivity, but its conductivity can be increased by the high physical interactions between polymer chains via hydrogen bonding between the hydroxyl groups and the doping metals; PVA is primarily dominated by the features of amorphous regions.[10–12] As an organic polymer nanocomposite, PVA is one of the most researched substances because of its numerous unique advantages, including its high solubility in water, non-toxic properties, wide crystallinity range and excellent film formation capability.[7,13–16]

The 2010 Nobel Prize in Physics was awarded to Andre Geim and Konstantin Novoselov because of their ground-breaking experiments regarding the 2D use of Gr as a monolayer of graphite (i.e., sp^2-hybridised carbon atoms) in pencils.[17] Gr exhibits unique behaviours both theoretically and experimentally, including high electron mobility (250,000 cm^2/Vs) at room temperature,[18,19] excellent thermal conductivity (5000 $Wm^{-1}\,K^{-1}$)[20] and superior mechanical properties.[21] The potential applications of these nanocomposites or nanoelectronics include solar cells (SCs), field-effect transistors,[22] light-emitting diodes,[23] super-capacitors[24,25] and lithium-ion batteries[26] as energy storage equipment and biosensors.[27]

On the contrary, one of the most important properties of Gr is its high electrical conductivity when used as a nanofiller within an insulating organic polymer matrix.[28] To explain the electrical conductivity of Gr as nanofiller, the percolation theory is frequently used. According to this theory, the percolation threshold of organic polymers, which depends on the size, shape and aspect ratio (AR) of nanofillers, can be decreased by using a larger AR and by effectively determining electrical conductivity.[29,30] Therefore, the conductivity of Gr-doped organic polymer nanocomposites can be substantially increased. When these nanocomposites are used as an interfacial layer between M and S, the MS structures are converted into MPS structures.[7]

Two methodologies are frequently utilised to evaluate the photovoltaic parameters of photodiodes or SCs. First, the short-circuit current (I_{sc}) for these devices is determined to achieve zero bias, and the open-circuit voltage (V_{oc}) is then contrarily determined at a zero current. Secondly, the photocurrents are changed depending on the polarity of the applied voltage via the illuminating condition when the devices are under polarised user reverse bias conditions, which is known as photoconductive analysis.[31] The photons, which are the fundamental particles of light and are related to the frequency and wavelength of electromagnetic waves, lead to the creation of electron–hole pairs in the depletion region of the S when it is exposed to photons whose energy values ($hc/q\lambda$) are higher than the energy band gap (E_g) of the S. The moving of the charged particles (i.e., electrons and holes) under the inner electric field regions of the S leads to a photocurrent in these devices.[31,32]

In this study, SJSs via non-doped and specific Gr-doped (1%, 3% and 7%) PVA layers were fabricated to investigate the basic electrical characteristics by using current–voltage (I–V) measurements under both forward and reverse bias conditions and distinct illumination levels at room temperature. The distinct doping concentration ratios of the Gr added to the PVA interlayers were produced by electrospinning and were utilised as an interfacial layer between Au and n-GaAs to evaluate the effect of the distinct doping concentration ratios. The primary objective of this study was to evaluate the potential use of Gr-doped PVA interlayers in photodiode applications.

EXPERIMENTAL PROCEDURES

After the wafer-cleaning processes explained by Çiçek et al.,[3,8] SJSs via non-doped and distinct Gr-doped (1%, 3% and 7%) PVA layers were prepared, as depicted by the schematic diagram presented in Fig. 1. The forward and reverse bias I–V measurements were performed using a Keithley 2400 source meter in dark conditions and under illumination at room temperature. The illumination of the samples was accomplished with a 250-W solar simulator (model: 69931 Newport-Oriel Instruments, Stratford, CT, USA), and the illumination intensity was measured by a radiometer. The photons at different power levels passed through an AM1.5 filter, which only allowed wavelengths between 400 and 700 nm to hit the diodes. All measurements were performed with the help of a microcomputer via an IEEE 488 AC/DC converter card in a Janes vpf-475 cryostat with four optic windows to avoid inference from external noise.

The electrospinning process utilised electrical force to produce polymer fibres, and the electrospinning setup consisted of four major components, including a high-voltage power supply (HVPS), spinneret, syringe pump and electrically conductive collector. In this system, by using a peristaltic syringe pump, the precursor solution was delivered with a metal needle syringe (10 ml) with an inner

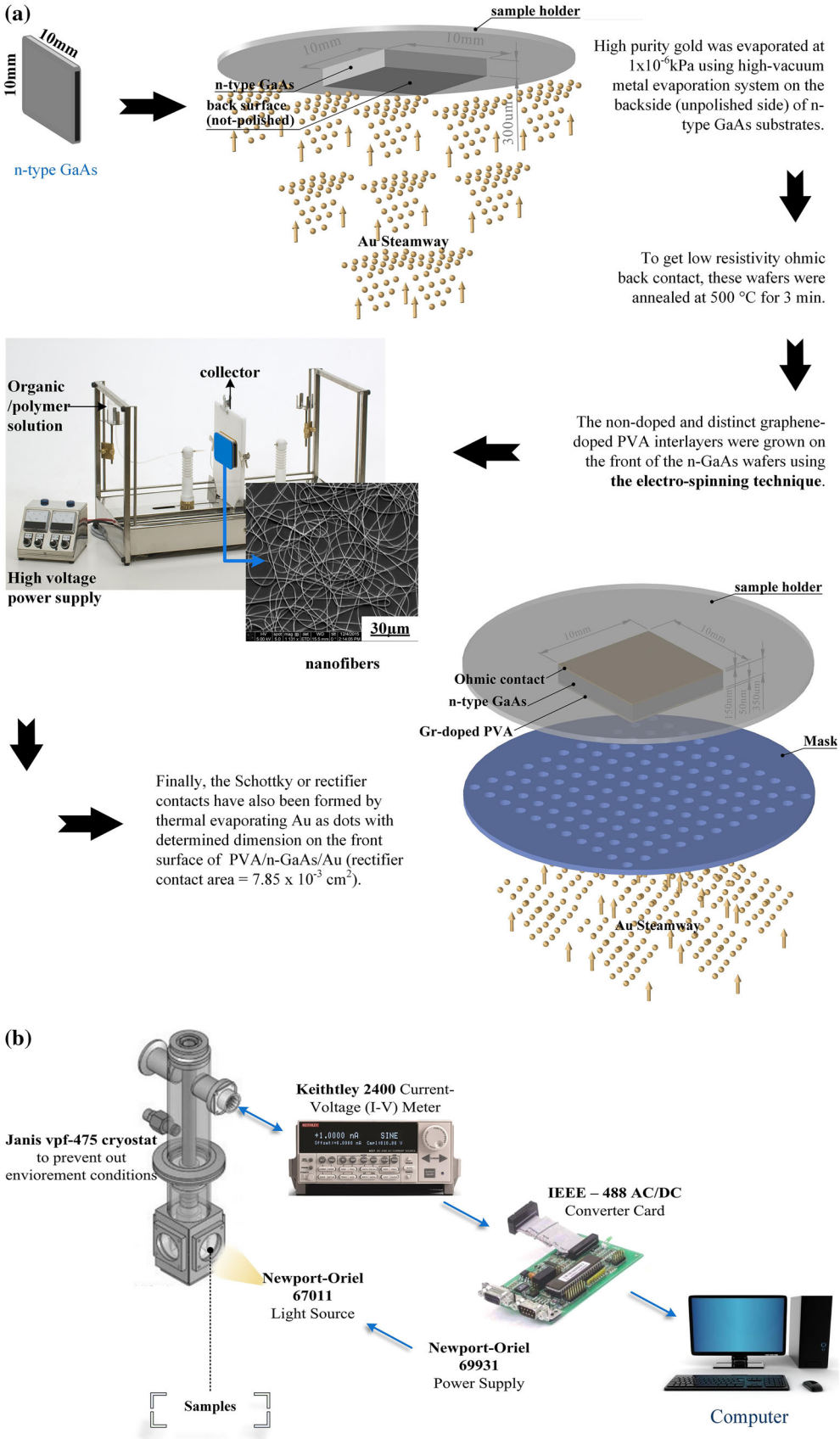

Fig. 1. Schematic diagram of preparation procedure (a) and measurement system (b) for SJSs via non-doped and distinct Gr-doped PVA layers.

diameter of 0.9 mm at a constant flow rate of 0.05 ml/h to deposit nanofibres onto substrates. The needle was connected to an HVPS and positioned vertically on a clamp. A piece of flat aluminium foil was placed 15 cm below the tip of the needle to collect the nanofibres, and a GaAs wafer was placed on the aluminium foil. Upon the application of a high voltage of 17 kV on the needle, a fluid jet was ejected from the tip. Non-doping and the distinct doping (1%, 3%, and 7%) PVA nanocomposite films were deposited onto the top-polished surface of the GaAs wafer by using the electrospinning technique. The scanning electron microscopy (SEM) images of the organic polymers (pure and 7% Gr-doped PVA) acetate nanofibres were presented in our previous study, where we successfully deposited them on the GaAs surface by using the electrospinning technique.[8]

RESULTS AND DISCUSSION

Compared with semiconductors, the major problems of pure polymer/organic materials include their lower carrier mobility and conductivity. To overcome these problems, pure polymer material is usually doped with a suitable dopant material such as cobalt, zinc, nickel or graphene. In this way, the doped organic interfacial layer causes improvements by ensuring lower series resistance (R_s), surface states (N_{ss}) and leakage current and higher charge storage. Therefore, in this study, various dopant concentrations (0%, 1%, 3%, 7% and 10%) of Gr-PVA interlayers were formed between Au and GaAs by using the electrospinning method to determine the best Gr doping concentration. The Au/(7% Gr-PVA)/*n*-GaAs (MPS) structure displayed the best performance. We observed that performance degradation began after Gr doping of 10% was used. The *I*–*V* characteristics of the non-doped PVA layers and the 1%, 3% and 7% Gr-doped PVA layers under dark conditions and distinct illumination levels investigated in both regions of forward and reverse biases are presented on a semilogarithmic scale (ln*I*–*V*) in Fig. 2. The illumination effect becomes prominent because of the increment increases in illumination levels, particularly in the non-doped structure under both reverse and forward bias conditions. This illumination effect almost loses its influence on the 1% and 3% Gr-doped structures, and the current levels in both biases were virtually the same. With respect to the 7% Gr-doped structure, the increment behaviour of reverse bias current with increasing illumination can be explained by photocell behaviour. Figure 2 clearly indicates that the 7% Gr-doped structure displayed good rectifying characteristics with lower reverse bias current and exponentially increased with a higher current at forward biases. Therefore, the 7% Gr-doped PVA layers displayed a higher rectifying ratio (RR = I_F/I_R) than the other structures. This also indicates that the 7% Gr-doped structure prevents the Io and increases the RR.

Usually, the main electrical parameters of the Schottky-type diode/photodiode and SCs were obtained/calculated from the forward bias *I*–*V* data on the basis of thermionic emission (TE) theory both in dark conditions and under various levels of illumination or radiation, particularly at or above room temperature. However, below room temperature, the thermionic field emission (TFE), field emission (FE) and Gaussian distribution of the barrier height model may be more effective than TE theory. Therefore, the Schottky formula was still valid for our measurements at room temperature. On the basis of the TE model, the relation between the current (*I*) and voltage (*V*) data can be derived by the equation below, which is closer to the ideal expression[33]:

$$I = I_o\left[\exp\left(\frac{q(V - \mathrm{IR_s})}{nkT}\right) - 1\right], \tag{1}$$

where parameters q, V, $\mathrm{IR_s}$, T and k can be expressed as the electron charges, the applied biases on the structure, the voltage drop on the R_s, the temperature in Kelvin and the Boltzmann constant, respectively. The voltage drop across the structure is equal to the difference between the total potential and voltage on the series resistance (*V*–IR) when $V > 3kT/q$. The ln*I*–*V* curves generally exhibit linear behaviour in the medium-voltage region and were investigated in three different regions as low, medium and high voltages. Here, the I_o can be extracted from the straight-line intercept of ln(*I*) at zero biases:

$$I_o = AA^*T^2 \exp\left(-\frac{q\Phi_{Bo}}{kT}\right), \tag{2}$$

where the rectifier contact area and the effective Richardson constant are denoted by A and A^* with values of 7.85×10^{-3} cm and 8.16 A/cm^2 K^2, respectively. The n values for these distinct Gr-doped MPS structures were realised in the medium-voltage region from the partial straight line of interception at the ln*I*–*V* plots and are expressed as follows:[33]

$$n = \frac{q}{kT}\left(\frac{\mathrm{d}V}{\mathrm{d}(\ln I)}\right), \tag{3}$$

The zero-bias barrier height Φ_{Bo} of each MPS structure can be derived by utilising the acquired saturation currents and rectifier contact area of the diodes together with the Richardson constant:

$$\Phi_{Bo} = \frac{kT}{q}\ln\left(\frac{AA^*T^2}{I_o}\right) \tag{4}$$

Table I shows the I_o, n and Φ_{Bo} values for non-doped and distinct Gr-doped structures.

The n values for every structure with non-doped and specific percentages of Gr-doped interlayers are greater than unity. For MPS-type SJSs, this can be

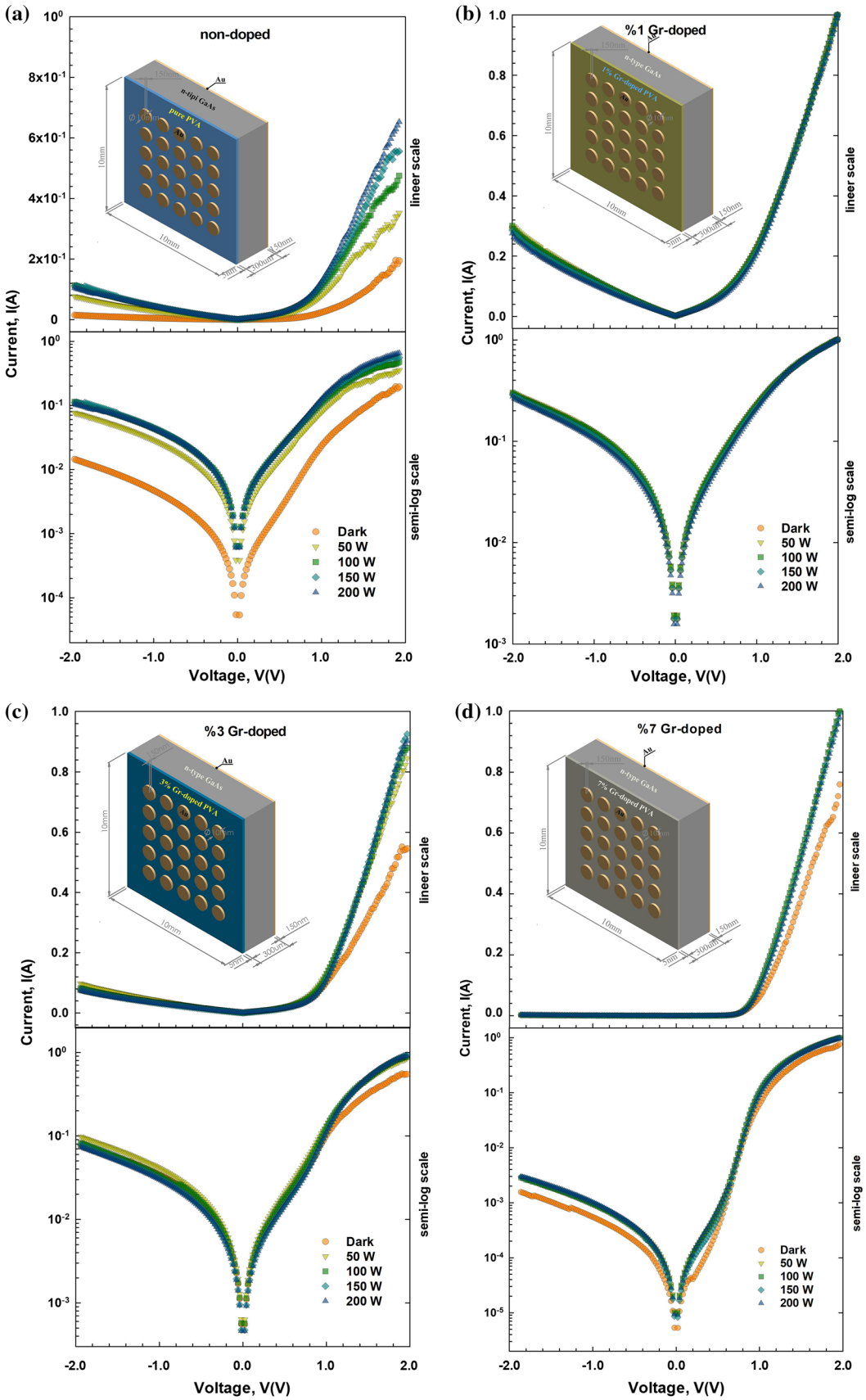

Fig. 2. The current–voltage (*I-V*) characteristics of SJSs via non-doped (a) and 1% (b), 3% (c) and 7% (d) Gr-doped PVA layers under dark and various illumination levels.

Table I. The basic electrical parameters for non-doped and distinct Gr-doped structures

	Non-doped			1% Gr-doped			3% Gr-doped			7% Gr-doped		
Power (*W*)	I_o **(mA)**	***n***	Φ_{Bo} **(eV)**	I_o **(mA)**	***n***	Φ_{Bo} **(eV)**	I_o **(mA)**	***n***	Φ_{Bo} **(eV)**	I_o **(μA)**	***n***	Φ_{Bo} **(eV)**
0	0.215	8.175	0.4260	10.662	11.888	0.3283	3.377	12.441	0.3571	13.50	6.675	0.4952
50	1.55	8.654	0.3765	11.810	12.141	0.3258	3.624	11.500	0.3553	35.40	6.753	0.4710
100	2.55	8.875	0.3640	11.408	12.114	0.3266	3.243	11.564	0.3581	36.20	6.776	0.4705
150	2.58	8.982	0.3638	10.523	11.996	0.3287	2.772	11.783	0.3620	28.30	6.941	0.4766
200	2.61	9.159	0.3635	9.451	11.891	0.3313	2.697	11.813	0.3627	27.50	6.953	0.4773

attributed to the presence of the interlayer, the interface thickness and distribution and the lateral inhomogeneous barrier height at the MS interface. It is also worth noting that the 7% Gr-doped structure displayed the lowest n and I_o values. On the contrary, when considering the variation ratio of the basic electrical parameter values, the 7% Gr-doped structure also displayed slightly higher Φ_{Bo} values than the other structures. This can be interpreted as the effectuality on the modification of the barrier height for the 7% Gr-doped structure being better than the other structures. The effects of R_s and R_{sh} on SJSs are very important in the determination of device performance and quality. The total voltage applied to the diodes is shared between the interfacial layer, the consumption layer and the resistances. Consequently, in addition to the existence of the interfacial layer, the R_s and R_{sh} values directly affect the device quality, performance and reliability.[34] Theoretically, the R_s value is presumed to be '0', and the R_{sh} value emerges to '∞'.

A curvature is seen in the high-voltage region because of the R_s value. Considering that the current reaches its saturation value, R_s increases by increasing the biases, and the curvature occurs because of the presence of R_s in this region. Parameters such as S resistivity, barrier height, front and back rectifier contacts, non-uniform interlayer, contacts of the probe wires and M/*S* interlayer impurities explain the origin of R_s.[33] The R_s values for SJSs can be calculated using different methods such as Ohm's law, Cheung and Cheung method and Norde method.[35,36] First, Ohm's law ($R_i = dV_i/dI_i$) was used to calculate R_s and R_{sh} from the forward and reverse biases of the *I–V* curve, respectively. Figure 3 presents the calculated R_s and R_{sh} values from Ohm's law of the non-doped PVA layers and the 1%, 3% and 7% Gr-doped PVA layers under dark conditions and distinct illumination intensities.

Figure 3 shows that the R_s values of the non-doped PVA interlayer structure are higher than the other structures under forward bias conditions. The illumination also influences the R_s value. Furthermore, the R_s values decrease as illumination intensity increases, particularly for the non-doped structure and at the least for the others (Fig. 3).

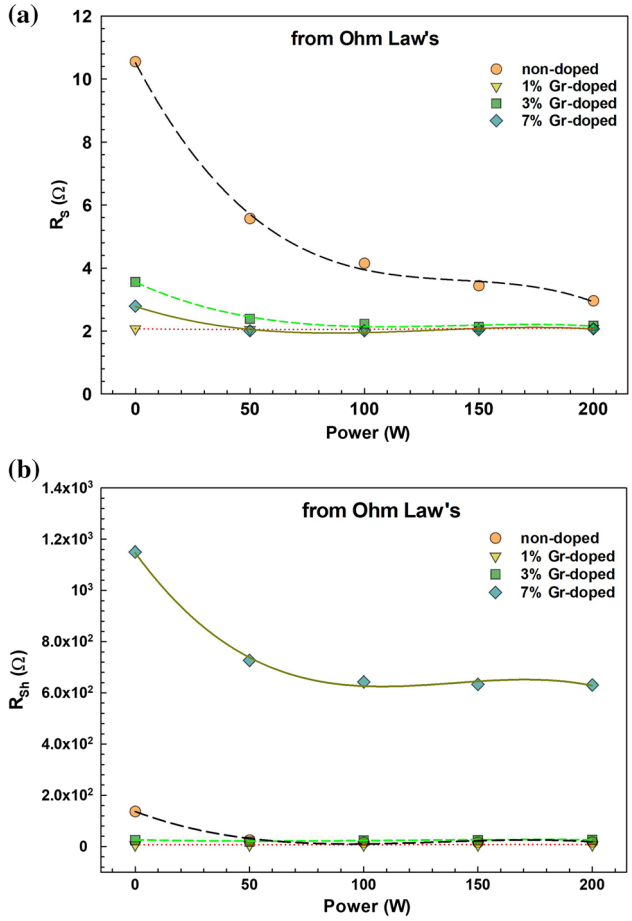

Fig. 3. The R_s (a) and R_{sh} (b) values obtained from Ohm's laws of SJSs via non-doped and distinct Gr-doped PVA layers under dark and various illumination levels.

However, the high reverse biases indicate that the R_{sh} values of 7% Gr-doped PVA layers are higher than the other structures and that it decreases prominently by illumination. In light of these two figures on R_s and R_{sh} versus illumination intensity, the lowest R_s and highest R_{sh} of the 7% Gr-doped PVA interlayer structure show that this structure is closer to the ideal behaviour than the other structures. This situation can also give an idea regarding

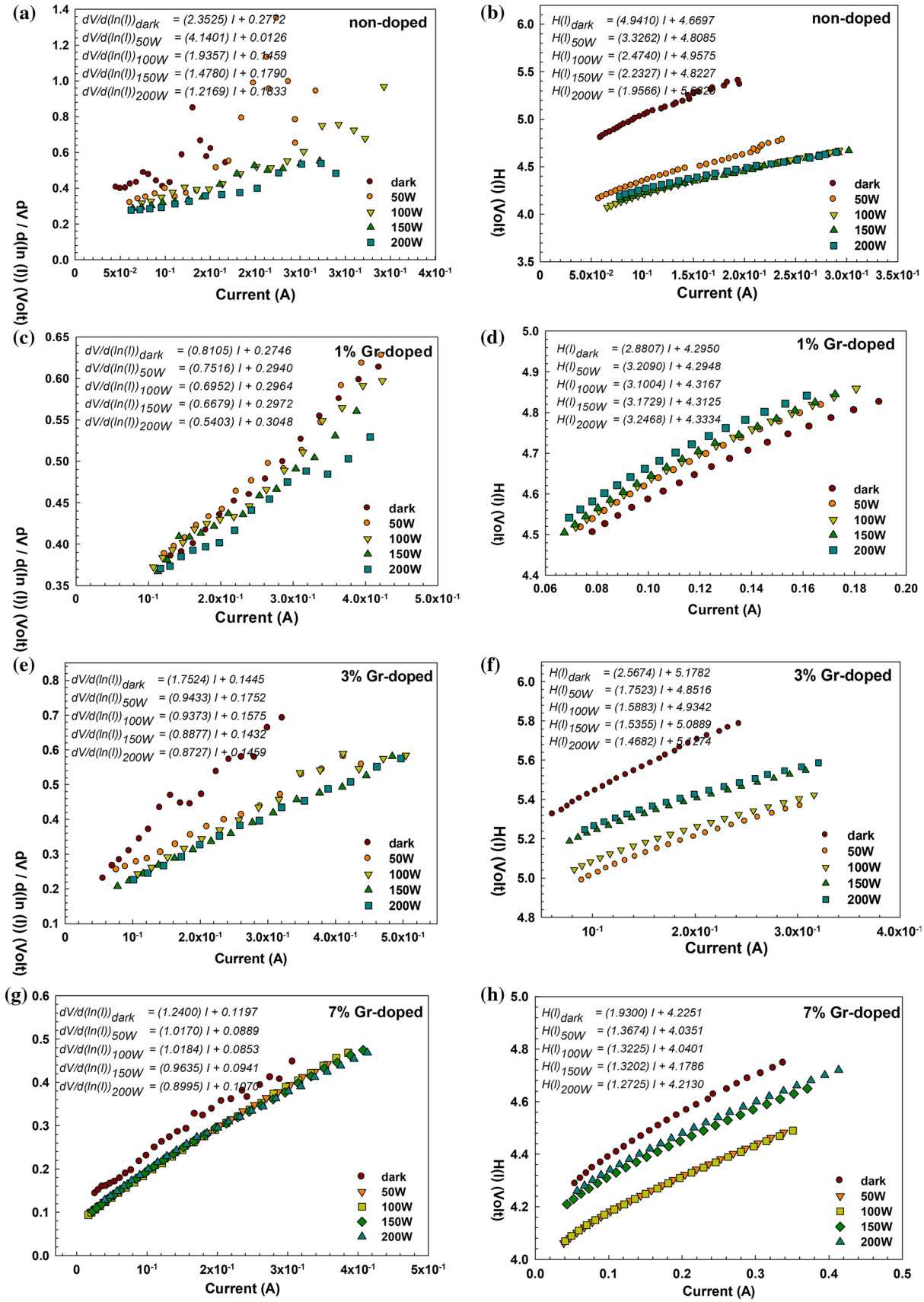

Fig. 4. The R_s values obtained from Cheung's function for SJSs via non-doped and distinct Gr-doped PVA layers under dark and various illumination levels.

Table II. The calculated R_s values from different methods for non-doped and distinct Gr-doped structures

Power (W)	From Ohm's law							From Cheung's function							
	R_s (Ω)				R_{sh} (Ω)			R_s (dV/dln$I$) (Ω)			R_s $H(I)$ – I (Ω)				
	Non-doped	1%	3%	7%	Non- doped	1%	3%	7%	Non-doped	1%	3%	7%	Non-doped	1%	3%	7%
0	10.55	2.07	3.56	2.79	137.63	7.19	26.21	1150	2.35	0.81	1.75	1.24	4.94	2.88	2.57	1.93
50	5.57	2.05	2.39	2.01	25.83	6.85	20.25	727.13	4.14	0.75	0.94	1.02	3.32	3.21	1.75	1.37
100	4.15	2.05	2.23	2.01	17.51	7.1	24.07	643	1.94	0.69	0.93	1.02	2.47	3.1	1.59	1.32
150	3.44	2.08	2.13	2.04	17.28	7.37	25.63	633.64	1.48	0.66	0.89	0.96	2.23	3.17	1.54	1.32
200	2.96	2.09	2.17	2.07	18.95	7.8	26.87	631.14	1.21	0.54	0.87	0.90	1.96	3.25	1.47	1.27

the RR of the structures, which can be derived by the ratio between forward bias current (I_F) and reverse bias current (I_R) as I_F/I_R. The combination of lower R_s values and highest R_{sh} value leads to better conductivity and rectifying properties and increases the RR for the 7% Gr-doped PVA interlayer structure.

Another way to determine the R_s values of Schottky diodes is by using the Cheung and Cheung method, which was acquired from a straight line positioned on the downward curve in the forward biases of the I–V plot.[35] Equations 5 and 6 refer to the Cheung functions from the literature:

$$\frac{dV}{d(\ln I)} = IR_s + \left(\frac{nkT}{q}\right), \tag{5}$$

$$H(I) = V - \frac{nkT}{q}\ln\left(\frac{I}{AA^*T^2}\right) = IR_s + n\Phi_{B0}. \tag{6}$$

Figure 4 shows the graphs for $dV/d\ln(I)$ and $H(I)$ versus the I of non-doped PVA interlayer MPS structures and 1%, 3% and 7% Gr-doped PVA interlayer MPS structures. Here, the x-axis (I) coefficient specifies R_s, and the y-axis interception specifies nkT/q and n at the $dV/d\ln(I)$ graphs. As shown in Fig. 4a–f, all graphs except for the 7% Gr-doped structure (Fig. 4g and h) show performance deterioration, which was interpreted from the lack of a linear shape. In other respects, complete cohesion was not acquired between the $dV/d\ln(I)$ and $H(I)$ functions, particularly for the 1% and 3% Gr-doped structures. The R_s values obtained from the $dV/d\ln(I) - I$ graph for 1% and 3% Gr-doped structures were lower than the values obtained from Ohm's law and the $H(I) - I$ graph. This is also an expected outcome that stems from factors such as rectifier contacts on both the front and back sides, non-uniform interlayer, barrier height and impurities between M/S interlayers. Table II shows the calculated R_s values from the different methods. Having a uniform distribution, lower series resistance values and highest shunt resistances make the 7% Gr-doped structure more optimal than the other structures evaluated in this study with respect to quality and reliability.

CONCLUSION

The I–V characteristics of non-doped PVA interlayers and 1%, 3% and 7% Gr-doped PVA interlayer MPS-type SJSs were investigated under both forward and reverse bias conditions and distinct illumination levels. The distinct doping concentration ratios of Gr added to the PVA interlayer were compared by taking into account the basic electrical parameters, including I_o, n, Φ_{Bo}, R_s and R_{sh}. The I_o values for the 7% Gr-doped structure were found to be the lowest under zero-bias conditions. It was also found that the 7% Gr-doped PVA decreased the n

value, but increased the Φ_{Bo} value compared with the values associated with the other structures. The R_s and R_{sh} values decreased as illumination levels increased. This finding is prominently seen from a comparison of the R_s values for the non-doped structure and the R_{sh} values of the 7% Gr-doped structure. By utilising Ohm's law and Cheung's functions, the R_s and R_{sh} values were obtained; in terms of quality and reliability, the 7% Gr-doped structure displayed better, uniformly distributed and lower R_s values and the highest R_{sh} values. In addition to having a better rectification ratio, the 7% Gr-doped structure displayed better quality because of its superior electrical properties compared with the other structures, thus making it a potentially attractive candidate for photodiodes in electronic devices.

ACKNOWLEDGEMENTS

This research was conducted as part of the comprehensive research project under contract numbers KU-BAP 01/2017-10, which is supported by Kastamonu University Scientific Research Project (KU-BAP), and GU-BAP.05/2018-10, which is supported by Gazi University Scientific Research Project. The authors would like to express their sincere appreciation for the contributions by KUBAP and GU-BAP.

REFERENCES

1. M. Soylu, A.A. Al-Ghamdi, and F. Yakuphanoglu, *Micro. Eng.* 99, 50 (2012).
2. Q. Zhang, V. Madangarli, M. Tarplee, and T. Sudarshan, *J. Electron. Mater.* 30, 196 (2001).
3. O. Çiçek, H. Uslu Tecimer, S.O. Tan, H. Tecimer, Ş. Altındal, and I. Uslu, *Composites Part B Eng.* 98, 260 (2016).
4. T. Tunç, Ş. Altındal, İ. Dokme, and H. Uslu, *J. Electron. Mater.* 40, 157 (2011).
5. I. Dökme, T. Tunç, I. Uslu, and Ş. Altindal, *Synth. Metals* 161, 474 (2011).
6. H. Uslu, Ş. Altındal, and İ. Dökme, *J. Electron. Mater.* 42, 2595 (2013).
7. S. Altındal Yerişkin, M. Balbaşı, and İ. Orak, *J. Mater. Sci. Mater. Electron.* 28, 14040 (2017).
8. O. Çiçek, H. Uslu Tecimer, S.O. Tan, H. Tecimer, İ. Orak, and Ş. Altındal, *Composites Part B Eng.* 113, 14 (2017).
9. H. Shirakawa, E. Louis, A. MacDiarmid, C. Chiang, and A. Heeger, *J. Chem. Soc. Chem. Com.* 1977, 578 (1977).
10. S. Demirezen, Ş. Altındal, and I. Uslu, *Curr. Appl. Phys.* 13, 53 (2013).
11. S. Alialy, H. Tecimer, H. Uslu, and Ş. Altındal, *J. Nanomed. Nanotechnol.* 3, 1 (2013).
12. H. Uslu, Ş. Altindal, and İ. Dökme, *J. Appl. Phys.* 108, 104501 (2010).
13. A.S. Roy, S. Gupta, S. Sindhu, A. Parveen, and P.C. Ramamurthy, *Composites Part B Eng.* 47, 314 (2013).
14. T. Tunç, İ. Uslu, İ. Dökme, Ş. Altındal, and H. Uslu, Inter. *J. Polym. Mater.* 59, 739 (2010).
15. S.B. Aziz, *J. Electron. Mater.* 45, 736 (2016).
16. S. Wageh, A.A. Al-Ghamdi, Y. Al-Turki, S.C. Tjong, F. El-Tantawy, and F. Yakuphanoglu, *J. Nanoelectron. Optoelectron.* 9, 678 (2014).
17. V. Singh, D. Joung, L. Zhai, S. Das, S.I. Khondaker, and S. Seal, *Prog. Mater Sci.* 56, 1178 (2011).
18. K.S. Novoselov, A.K. Geim, S.V. Morozov, D. Jiang, M.I. Katsnelson, I.V. Grigorieva, S.V. Dubonos, and A.A. Firsov, *Nature* 438, 197 (2005).
19. K.S. Novoselov, A.K. Geim, S.V. Morozov, D. Jiang, Y. Zhang, S.V. Dubonos, I.V. Grigorieva, and A.A. Firsov, *Science* 306, 666 (2004).
20. A.A. Balandin, S. Ghosh, W. Bao, I. Calizo, D. Teweldebrhan, F. Miao, and C.N. Lau, *Nano Lett.* 8, 902 (2008).
21. C. Lee, X. Wei, J.W. Kysar, and J. Hone, *Science* 321, 385 (2008).
22. M. Rahmani, H. Ghafoori Fard, T. Ahmadi, S. Rahbarpour, H. Habibiyan, V. Varmazyari, and K. Rahmani, *J. Electron. Mater.* 46, 6188 (2017).
23. M. Yazdan Mehr, S. Volgbert, W.D. van Driel, and G.Q. Zhang, *J. Electron. Mater.* 46, 5866 (2017).
24. S. Konwer, R. Boruah, and S. Dolui, *J. Electron. Mater.* 40, 2248 (2011).
25. C. Liu, Z. Yu, D. Neff, A. Zhamu, and B.Z. Jang, *Nano Lett.* 10, 4863 (2010).
26. N. Li, Z. Chen, W. Ren, F. Li, and H.-M. Cheng, *PNAS* 109, 17360 (2012).
27. N.F. Atta, A. Galal, and E.H. El-Ads, *Graphene: nanotechnology and nanomaterials: biosensors—micro and nanoscale applications* (Croatia: IN TECH, 2015), p. 37.
28. D. Galpaya, M. Wang, M. Liu, N. Motta, E. Waclawik, and C. Yan, *Graphene* 1, 30 (2012).
29. T.N. Zhou, X.D. Qi, and Q. Fu, eXPRESS Polym. *Lett.* 7, 747 (2013).
30. S.M. Zhang, L. Lin, H. Deng, X. Gao, E. Bilotti, T. Peijs, Q. Zhang, and Q. Fu, *Express Polym. Lett.* 6, 159 (2012).
31. M. Yıldırım, *Thin Solid Films* 615, 300 (2016).
32. B.L. Sharma, *Metal-semiconductor Schottky barrier junctions and their applications* (New York: Plenum Press, 1984).
33. E. Rhoderick and R. Williams, *Metal-semiconductor contacts* (Oxford: Oxford University Press, 1978).
34. M. Gökçen, Ş. Altındal, M. Karaman, and U. Aydemir, *Phys. B Condens. Matter.* 406, 4119 (2011).
35. S.K. Cheungve and N.W. Cheung, *Appl. Phys. Lett.* 49, 85 (1986).
36. H. Norde, *J. Appl. Phys.* 50, 5052 (1979).